Composite Materials
2025, Vol. 9, No. 1, pp. 18-27
https://doi.org/10.11648/j.cm.20250901.12

Research Article

Orbital Hybridation-Driven Selective Adsorption in Cr-Doped C_3N_2 Monolayers: A DFT Exploration for High-Performance Insulating Gas Sensing

Tao Wang[1], Xuchu Hu[1], Huan Yang[1], Lei Chen[1], Jianjun Cao[2, *], Pengfei Jia[2], Yiyi Zhang[2]

[1]Guangxi Liuzhou Special Transformer Co., Ltd., Liuzhou, China

[2]School of Electrical Engineering, Guangxi University, Nanning, China

Abstract

This study uses first-principles DFT to investigate the regulatory mechanism of Cr doping on C_3N_2 monolayer adsorption of CH_4, CO_2, and C_2N_2. Results show Cr atoms stably incorporate into C_3N_2 pore sites (binding energy: -4.26 eV), altering electronic properties via Cr-3d/N-2p hybridization. Adsorption analyses reveal selective capture: C_2N_2 shows strong chemisorption via Cr-N covalent bonding (E_{ads}: -2.148 eV, ΔQ: -0.034 e), CO_2 moderate adsorption via Cr-O polar interactions (-0.866 eV, -0.082 e), and CH_4 physical adsorption (-0.305 eV, 0.004 e). Density of states analysis clarifies hybridization mechanisms, while work function calculations show a 9.2% increase upon C_2N_2 adsorption, confirming its potential as a gas sensor. This work provides a novel 2D nitride design for insulation fault gas detection and advances understanding of gas-sensitive interfacial interactions.

Keywords

Cr-C_3N_2, Insulating Decomposition Gases, Selective Adsorption, DFT

1. Introduction

With the development of power systems towards high voltage and large capacity, the safety of gas-insulated equipment (e.g. GIS, GIL) has become a key issue [1, 2]. The internal insulating materials of the equipment may decompose under high voltage or partial discharge conditions to produce characteristic gases such as CH_4, CO_2, C_2N_2, etc [3, 4]. The accumulation of these gases not only accelerates the aging of the insulation, but also triggers equipment failure [5, 6]. The development of highly sensitive and selective gas adsorption materials is of great significance in realizing early failure warning and condition monitoring. Two-dimensional materials (e.g., graphene, C_3N_2 monolayer) show potential in the field of gas sensing and adsorption due to their large specific surface area and tunable electronic properties [7]. However, the original C_3N_2 monolayer has limited adsorption capacity for some non-polar or weakly polar gases, and modulation of its surface active sites by transition metal doping can significantly enhance the gas adsorption performance and provide a novel solution for gas monitoring in high-voltage insulating equipment [8, 9].

In recent years, two-dimensional carbon nitride materials (C_3N_2 C_3N_4) have been widely investigated due to their

*Corresponding author: cjj2321704917@163.com (Jianjun Cao)

Received: 22 May 2025; **Accepted:** 9 June 2025; **Published:** 23 June 2025

unique semiconducting properties [10], but relatively few theoretical explorations have been carried out for C_3N_2 monolayers. It has been shown that metal doping (Fe, Co) can enhance the interaction between the material and gas molecules by introducing localized density of states and charge transfer [11]. However, most of the existing studies focus on common gases (e.g., NO_2, NH_3), and the adsorption mechanism of high-pressure insulating decomposition gases (especially C_2N_2) is not clear. In addition, how to balance the adsorption strength and selectivity by precisely tuning the doping sites and concentrations remains a challenge [12-14].

Chromium atoms, with their diverse electronic structures, adsorption control capabilities, structural compatibility, and cost advantages, have emerged as "multifunctional atoms" in material doping and modification. From electronic devices to catalytic systems, and from structural materials to functional coatings, chromium doping not only optimizes the intrinsic properties of the substrate but also endows materials with new physical and chemical characteristics, making it indispensable in fields such as energy, electronics, and aerospace. For example, Zhao et al [15]. utilized Cr atom doping in WS_2 for the adsorption treatment of harmful gases in agricultural greenhouses, highlighting the electronic property regulation mechanism of Cr atoms on intrinsic WS_2.

In this study, first-principle density functional theory (DFT) is employed to systematically investigate the effects of Cr atom doping on the electronic structure and gas adsorption properties of C_3N_2 monolayers. The interaction mechanisms of Cr doping sites with CH_4, CO_2, and C_2N_2 molecules are revealed by calculating the adsorption energy, charge transfer, density of states (DOS), and work function. To explore the differences in the adsorption configurations of the three gases on the Cr-C_3N_2 surface and how Cr doping alters the surface charge distribution and active site properties of the C_3N_2 monolayer. The theoretical basis for the selective adsorption of multi-component gases is provided by the electronic structure modulation strategy. The results can provide theoretical guidance for the design of new gas sensors or adsorbents, and promote the development of intelligent monitoring technology for high-voltage electrical equipment.

2. Experimental Methods

All calculations on DFT are based on the MS software Dmol3 module, and the calculations are performed using a 128-core processor. The system structure optimization is performed using the PBE generalization in the generalized gradient approximation [16, 17], the weak interaction correction is performed using DFT-D3 [18-20], and the bi-numerical basis group DNP with file version 3.5 is chosen to improve the accuracy of the calculations [21, 22]. The SCF convergence is set to 1.0×10^{-5}, the specific number of loops is set to 500, the hot-tail smearing effect smeaning is set to 0.005 [23, 24], and the size of the DIIS is set to 6 in order to accelerate the efficiency of electronic structure calculation. A $2 \times 2 \times 1$ supercellular C_3N_2 monolayer structure was constructed, and the vacuum layer was set to 25 Å to avoid cyclic effects [25-27].

The magnitude of adsorption energy between gas molecules and adsorption substrate is calculated as shown in Equation (1).

$$E_{\text{ads}} = E_{\text{total}} - (E_{\text{surface}} + E_{\text{gas}}) \tag{1}$$

In In Equation (1) E_{ads} is the adsorption energy, E_{total} is the total energy of the system after adsorption, E_{surface} is the energy of the adsorbent [28], and E_{gas} is the energy of the adsorbed target gas. The adsorption energy is similar to the binding energy, and the larger the absolute value is, the stronger the interaction between the two systems is when it is negative [29]. We expect the adsorption energy to have a suitable size to meet the subsequent sensing requirements.

In gas adsorption, transfer of charge (ΔQ) refers to the phenomenon of transfer and rearrangement of electrons between a gas molecule and a solid surface [30, 31]. The size of the transferred charge often determines the bonding between the adsorbed molecule and the adsorbent, and the formula for calculating the transferred charge is as follows:

$$Q_i^{Hirshfeld} = \int \rho_{total}(\mathrm{r})\pi_i(\mathrm{r})d\mathrm{r} - Z_i \tag{2}$$

$$Q_i^{Mulliken} = \frac{1}{2}N_i + \sum_{j\neq i} P_{ij} \tag{3}$$

$$Q_{transfer} = \sum_i (Q_{i,final} - Q_{i,initial}) \tag{4}$$

Equations (2) and (3) are the Milligan and Hashfield charge calculations, respectively. In Equation (2), $Q_i^{Mulliken}$, N_i and P_{ij} denote the charge of atom i, the number of atoms i and the Overlap integral between atoms i and j, respectively, and the calculation depends on the orbital overlap between them. In Equation (3) $Q_i^{Hirshfeld}$ denotes the charge of atom i, $\rho_{total}(\mathrm{r})$ is the total electron density, $\pi_i(\mathrm{r})$ is the electron distribution function of atom i, and Z_i is the atomic number of the nucleus. Equation (4) shows the calculation formula before and after transfer charge adsorption, where $Q_{i,initial}$ is the total number of charges before adsorption of the system and $Q_{i,final}$ is the total number of charges after adsorption of the system, and the number of transferred charges is obtained by doing the difference. Where the positive and negative of the transfer charge represents the transfer direction.

Work function (W_ϕ) is the minimum energy required to move an electron from the Fermi level of a solid material into a vacuum [32, 33]. It is an important parameter to characterize the electron energy level on the surface of a material, and is calculated as:

$$W_\phi = E_F - E_0 = -\frac{1}{e}\int_0^{E_F} g(E)dE \tag{5}$$

where E_F is the Fermi energy level, E_0 is the vacuum en-

ergy level, and W_ϕ is the work function. In the integral expression, e is the charge of a single electron (about 1.602×10^{-19} C) [34], and $g(E)$ is the energy density of states, which indicates the number of available electronic states per unit energy range, depending on the structure of the material and the distribution of electronic states.

3. Results and Discussion

3.1. Effect of Cr Doping on the Structure and Electronic Properties of C_3N_2

The introduction of Cr atoms causes large changes to the microscopic surface structure as well as the electronic structure of the system. Figures 1(a) and (b) show the schematic structures of C_3N_2 and Cr-C_3N_2 monolayers, respectively. Observation reveals that C_3N_2 as a whole exhibits a symmetric circular pore-like structure, and interestingly, we find that this symmetry is not broken when Cr atoms are introduced into the system. In addition, in order to find the optimal doping sites, we have tested the doping of common alternative doping sites (N and C), both top and bridge sites, and the results show that the pore doping system has the optimal performance with a binding energy of -4.26 eV, which is also in agreement with the previous studies of many scholars [35, 36].

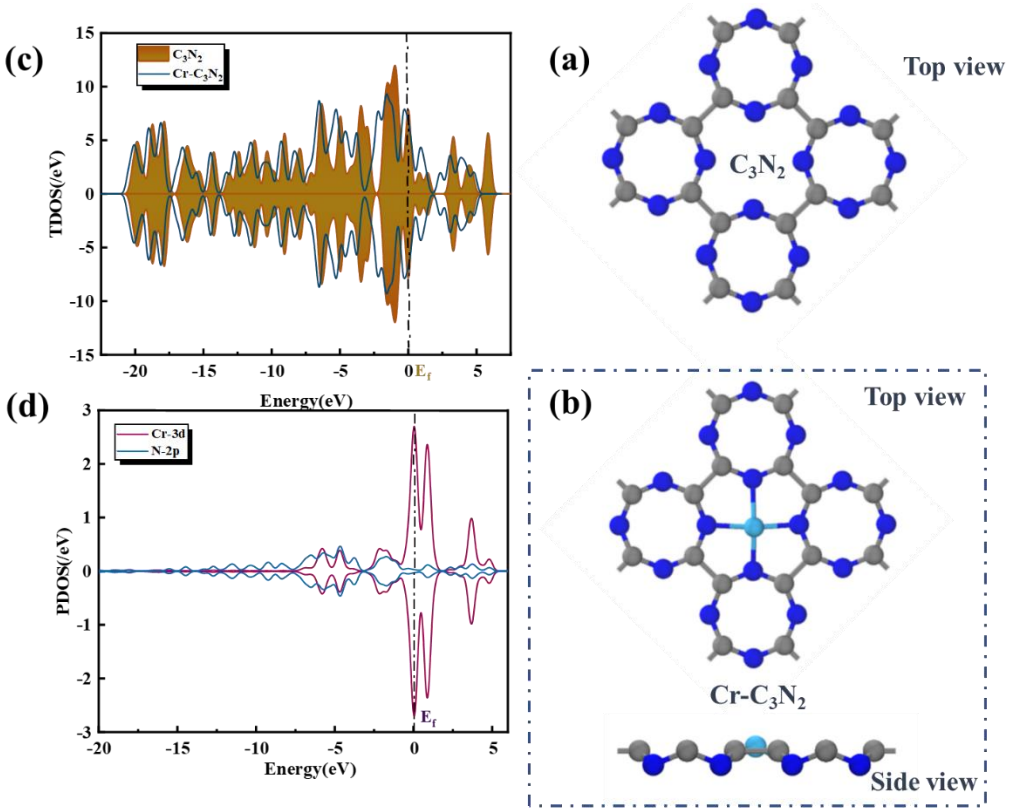

Figure 1. *Density of states and structure schematic. (a) Schematic structure of C_3N_2; (b) Schematic structure of Cr-C_3N_2; (c) C_3N_2 and Cr-C_3N_2 total density of states; (d) Cr and N projected density of states.*

Comparing the density of states before and after doping, the DOS near the Fermi energy level (0 eV) is significantly enhanced (with a pronounced peak), suggesting that doping of Cr atoms has led to the emergence of new electronic states of the material at the Fermi energy level. This may lead to a reduced band gap, easier electronic excitation of the material, and enhanced conductivity [37], suggesting a possible transition of the material from a wide band gap semiconductor to a narrow band gap semiconductor. -7.5 ~0 eV region (near the top of the valence band), after Cr doping, the DOS is more localized near the top of the valence band, and it is not difficult to find out by observing the density of the fractional-wave states that this phenomenon originates from the hybridization of the 3d orbitals of Cr with the N-2p orbitals. In addition, the strong peaks near the Fermi energy level in the PDOS diagram indicate that the Cr-3d orbitals are directly involved in the electron transport in their vicinity, which is the main source of the enhanced conductivity of the material [38]. Moreover, in the valence band from -7.5 to -3 eV and the conduction band from 2.5 to 6 eV, hybridization between the N-2p orbitals and the Cr-3d orbitals occurs, suggesting the formation of N-Cr bonds.

3.2. Exploration of CH_4, CO_2 and C_2N_2 Adsorption on Cr-C_3N_2 Surface

In order to analyze the adsorption properties of the three gases on the surface of Cr-C_3N_2 monolayer membrane structure, the adsorption model of each gas was firstly established as shown in Figure 2. The calculated results show that there are significant differences in the adsorption capacities of Cr-C_3N_2 for the three gases, with the adsorption strengths in the order of C_2N_2 > CO_2 > CH_4, corresponding to adsorption energies of -2.148 eV, -0.866 eV, and -0.3045 eV, respectively. mong them, the adsorption distance of C_2N_2 was the shortest (1.933 Å) with the strongest adsorption energy, which suggesting the formation of a strong chemical interaction with the Cr active site, possibly originating from the hybridization of the N atoms in the C_2N_2 molecule with the Cr-3d orbitals (the tight adsorption configuration in the top view further supports this conclusion). In contrast, CH_4 has a larger adsorption distance (4.138 Å) and a weaker adsorption energy, suggesting that its adsorption mode is dominated by physical adsorption related to van der Waals interactions on the surface of the Cr-C_3N_2 [39]. The adsorption behavior of CO_2 is intermediate between the two (adsorption distance of 2.302 Å), which is presumed to achieve a moderate strength of adsorption through partial charge transfer between the O atoms and the Cr sites. adsorption. In addition, the adsorption data were recorded in Table 1.

Table 1. *Comparison of various calculated data for Cr-C_3N_2@X.*

System (doping modification)	W_ϕ (Ha)	E_{ads} (eV)	ΔQ (e)	Distance (Å)	Structure
Cr-$C_3N_{2@}CO_2$	0.187	-0.866	-0.047	2.302	Figure 2(c)
Cr-$C_3N_{2@}CH_4$	0.196	-0.305	-0.004	4.138	Figure 2(b)
Cr-$C_3N_{2@}C_2N_2$	0.213	-2.148	-0.034	1.933	Figure 2(a)

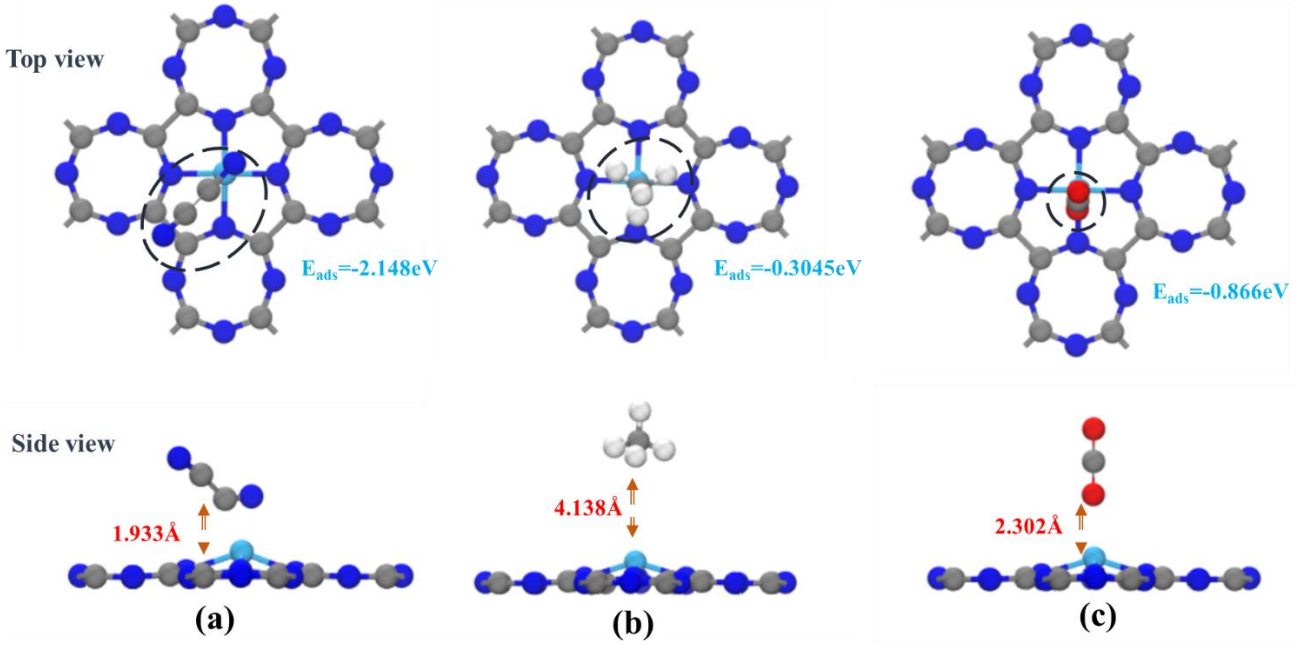

Figure 2. *Schematic diagram of CH_4, CO_2, C_2N_2 adsorption structure.*

Differential electron density can better analyze the nature of interfaces or interatomic interactions [40], for which we plotted the total and differential electron density maps of the three adsorption models (Figure 3), in which the isosurfaces in the total electron density map are more uniformly distributed, and do not have a large color difference, and the three adsorption systems transfer charges of C_2N_2 (-0.034 e), CH_4 (-0.004 e) and CO_2 (-0.082 e). The differential electron densities show that in C_2N_2, the yellow region (electron accumulation) is concentrated between Cr and N atoms, and the blue region (electron depletion) is located around Cr atoms, suggesting that the charge is transferred from Cr to the adsorbed molecules, which may form partial ionic bonds. For CH_4, the region between the gas and the substrate has almost

no significant yellow/blue region and the charge transfer is negligible, corroborating its physical adsorption properties. In the CO_2 adsorption system, the red region surrounds the lowermost C atom while the blue region extends up to the Cr atom, suggesting that Cr serves as an electron donor and the electrons are transferred from the substrate to the gas. Interestingly, however, a region with no obvious color intermingling remains between the two atoms, suggesting that CO_2 adsorption may be an interaction between chemisorption and physisorption [41]. Based on the above analysis, the unique electron-donor property of Cr atoms makes them exhibit selective adsorption on C_2N_2, which provides a theoretical basis for the design of efficient gas separation and sensing materials.

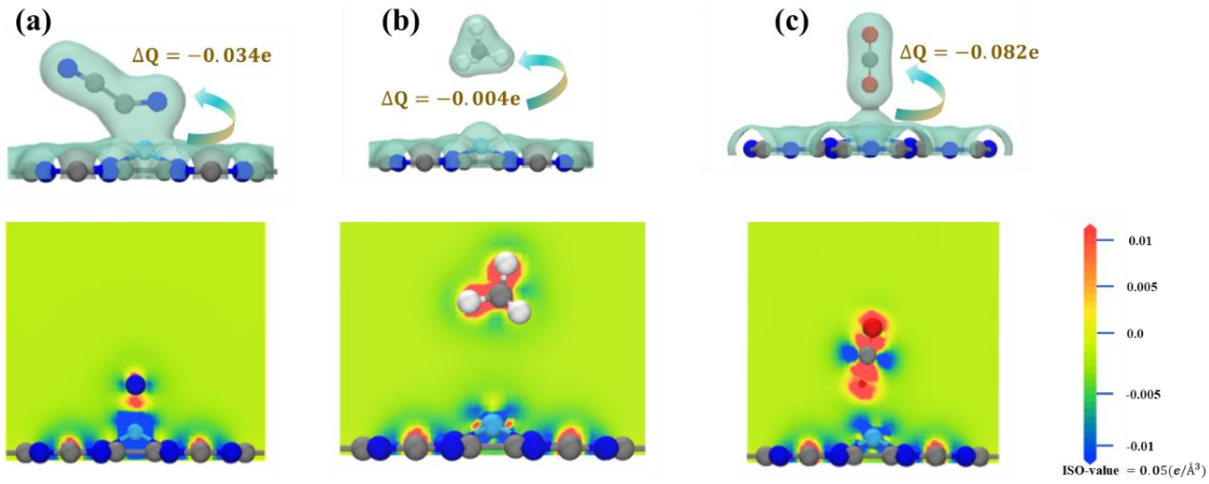

Figure 3. *Electron cloud density in adsorption systems. (a) C_2N_2; (b) CH_4; (c) CO_2.*

3.3. Electronic Structure Reconstruction and Work Function Regulation Mechanism of Cr-C_3N_2 Gas-sensitive Interfaces

The PDOS and TDOS of Cr-C_3N_2@X (X = CO_2, CH_4, and C_2N_2) are shown in Figure 4. It should be noted that the adsorbed gases (CH_4, C_2N_2, and CO_2) significantly altered the density of states on the right-hand side of the Fermi energy level (Figure 4a-c) for Cr-C_2N_2, and the different gases induced a unique TDOS response. the TDOS peaks near the Fermi energy level for Cr-C_3N_2@C_2N2 TDOS peaks near the Fermi energy level are significantly enhanced and new localized states appear from -2 to 0 eV, indicating that C_2N_2 adsorption induces a strong hybridization of Cr-3d with N-2p. The TDOS peaks at the Cr-C_2N_2@CO_2 Fermi energy level are slightly decreased, but new peaks appear from 2.5 to 1 eV, which corresponds to the hybridization of O-2p with Cr-3d and leads to partial charge transfer (Cr → O). A non-negligible point is that the TDOS of the system does not show symmetry after adsorption of CO_2 and CH_4, which may be related to the fact that the adsorption leads to different density distributions of spin-up (↑) and spin-down (↓) states of the Cr-3d orbitals (e.g., the spin-up↑ state is more localized near the Fermi energy level), which results in the breaking of the positive and negative symmetry of the TDOS. This asymmetry not only reflects the reconfiguration of the electronic structure, but may also suggest that the material has new functional properties (e.g., catalytically active sites or selective adsorption capacity) upon adsorption [42].

PDOS further reveals the orbital hybridization mechanism and charge transfer pathways. In the Cr-C_3N_2@C_2N_2 system, Cr-3d, N-2p, and C-2p show strong hybridization peaks (>60% of the integral area of the overlap region) at -7.5 to -2.5 eV, suggesting that the gas strongly interacts with the substrate atoms, which is in agreement with the previous analysis. In the Cr-C_3N_2@CO_2 (Figure 4d), the O-2p orbitals and the Cr-3d orbitals show overlap phenomena in the conduction band region 2.5 to 5 eV, emphasizing the obvious charge transfer and possessing weak chemisorption characteristics. In the CH_4 system, the PDOS of H-1s (green) appears as a weak peak at -6 to -4 eV, and the overlap region with Cr-3d has a smaller area, indicating that the H atoms are not directly involved in the bonding of Cr, and may act as surface protons or adsorption sites to bridge molecules, and the gas-substrate interaction mainly The gas-substrate interaction is mainly characterized by physical adsorption [43]. In addition, the Cr-3d orbital PDOS of the CO_2 and CH_4 systems show asymmetric features that match those in TDOS. This suggests that after adsorption of these two gases on the substrate, there are unpaired electrons in the 3d orbitals of Cr^{3} (d^{3}electronic configuration), and the density responses of the spin-up (↑) and spin-down (↓) states are different after adsorption, with the spin ↑ state of the Cr atom localized at 2 eV in Cr-C_3N_2@CO_2 and the peaks are more acute. The spin ↓ state is dispersed in a wider energy range (-2.5~0 eV) with a lower peak intensity, resulting in an asymmetric total PDOS.

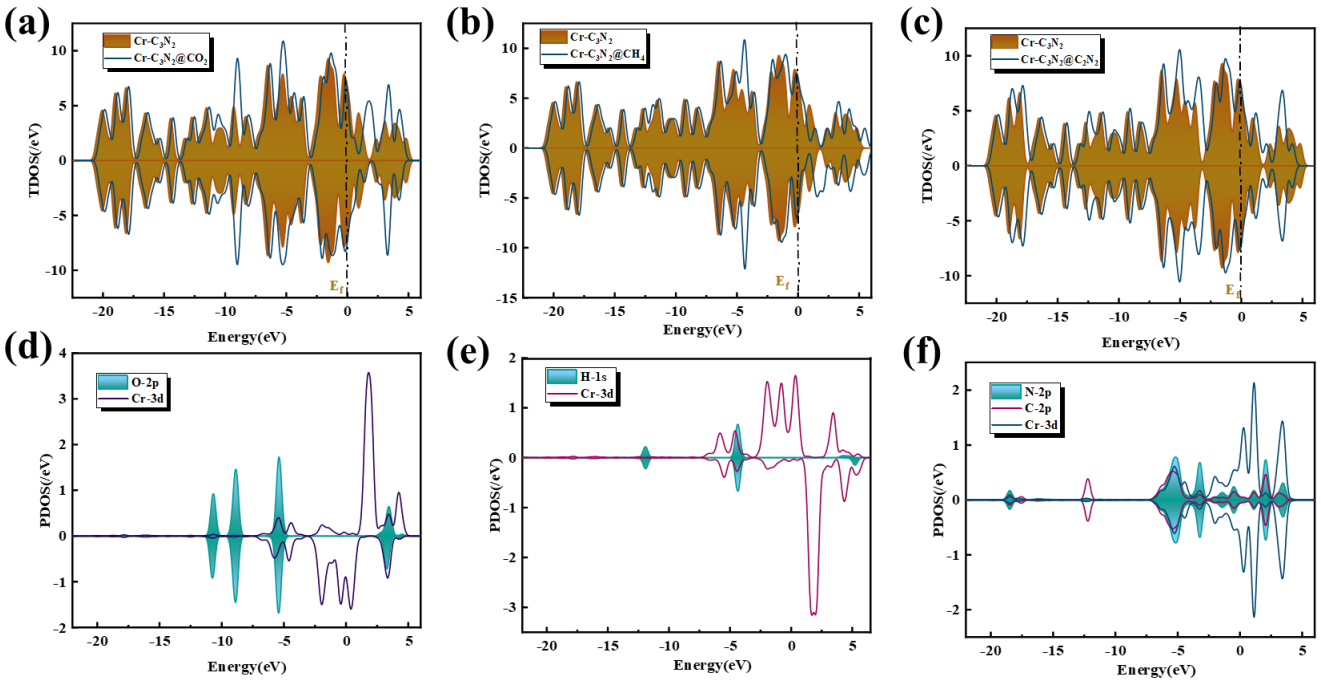

Figure 4. *TDOS and PDOS for each adsorption system. (a, d) CO_2; (b, e) CH_4; (c, f) C_2N_2.*

Based on the electronic density analysis discussed earlier, it is evident that the hybridization effect between the Cr-3d orbital and the N atomic orbital in the C_2N_2 gas is the most significant. This is essentially the result of the synergistic interaction between their electronic structures, energy matching, and bonding requirements. The multi-valent orbitals of Cr and the lone pair electrons of N form efficient overlap through hybridization. Additionally, the difference in electronegativity and the diversity of coordination numbers further promote the formation of hybridized orbitals. This characteristic holds significant application value in fields such as coordination chemistry.

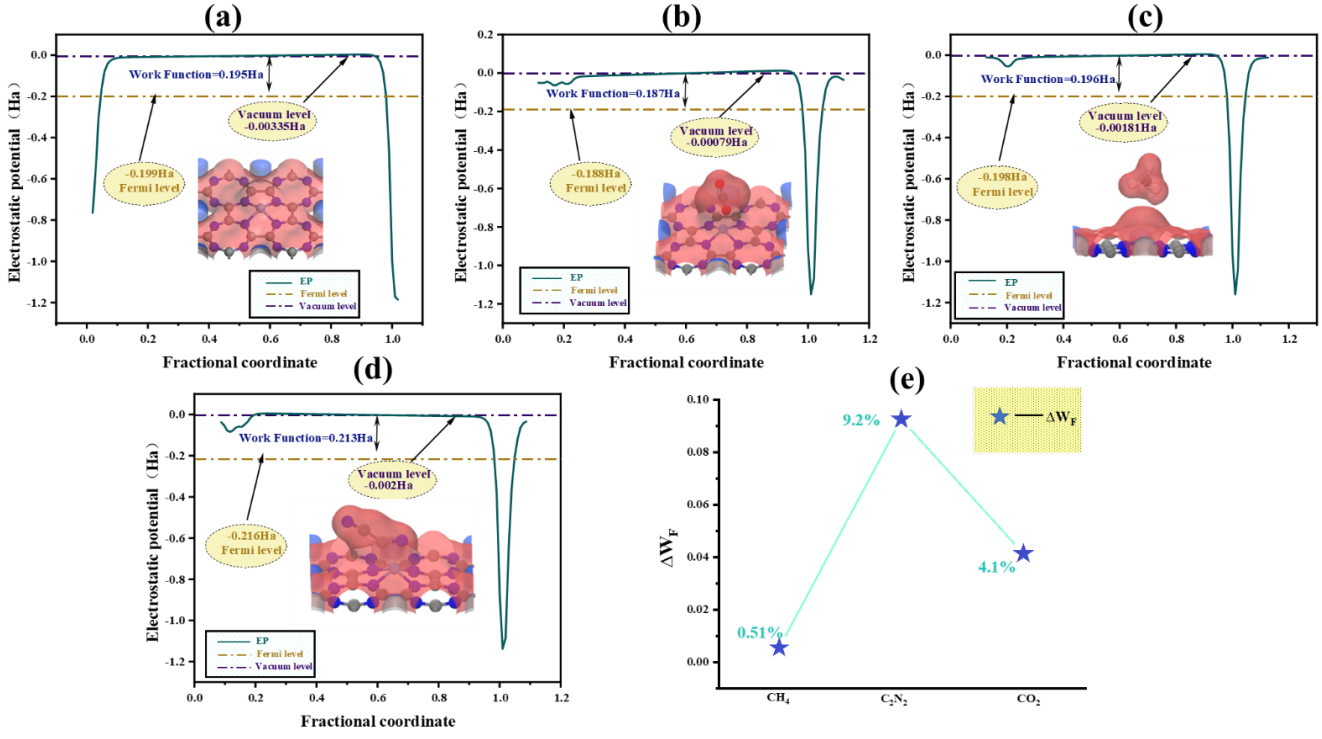

Figure 5. *Rates of change of work function, electrostatic potential and work function before and after Cr-C_3N_2 adsorption. (a,) Cr-C_3N_2; (b) Cr-C_3N_2@CO_2; (c) Cr-C_3N_2@CH_4; (d) Cr-C_3N_2@C_2N_2; (e) Rates of change of work function.*

The electrostatic potential (EP) distribution and work function (W_F) calculations systematically reveal the regulation laws of surface electron escape behavior in the Cr-C_3N_2 material after adsorbing CO_2, CH_4, and C_2N_2 gas molecules. As shown in Figures 5(a)-(d), the difference between the vacuum level and the Fermi level of the pristine Cr-C_3N_2 corresponds to a work function WF of 0.195 Ha (≈5.30 eV). After gas adsorption, the work function exhibits significant evolutionary differences: the work function of the C_2N_2 adsorption system increases substantially to 0.213 Ha (≈5.80 eV, ΔWF=+9.2%), enhancing the surface electron escape barrier. Additionally, the work functions of the CO_2 and CH_4 adsorption systems change from 0.195 Ha to 0.187 Ha (-4.2%) and 0.196 Ha (+0.51%), respectively. Notably, in the CO_2 system, O acts as an electron acceptor to acquire a small amount of electrons from Cr, which reduces the surface potential (the vacuum level rises relatively, but the amplitude is smaller than that of the Fermi level rise) [44], leading to a decrease in the system work function. The slight increase in the work function of the CH_4 system may be due to the fact that the weak polarization of the gas induces an instantaneous dipole on the surface [45], slightly reducing the electron density at the Cr sites, but there is no significant charge transfer (ΔQ≈0). The Fermi level rises slightly due to the minor perturbation of the substrate's electronic structure, resulting in a small increase in the work function. Based on the above comprehensive analysis, the work function enhancement effect induced by C_2N_2 adsorption indicates that Cr-C_3N_2 can serve as a work function-type sensing device for C_2N_2, as well as an oxidation-resistant coating or electrochemical catalytic interface suitable for inhibiting electron migration. This study provides a theoretical framework and design strategy for precisely regulating the electron escape characteristics of low-dimensional nitrides through molecular adsorption.

Table 2. *Comparison with previous work.*

Gas type	Sensing material	E_{ads} (eV)	Ref.
CO_2	Cr-C_3N_2	-0.866	Our work
C_2N_2	Cr-C_3N_2	-2.148	
CH_4	Cr-C_3N_2	-0.305	
CO_2	Pt-C_3N_2	-0.214	[46]
C_2N_2	Pt-C_3N_2	-0.1	
CH_4	Pt-C_3N_2	-0.096	

Table 2 provides a detailed comparison with previous work. It is not difficult to see that after doping with Cr atoms, the adsorption characteristics of C3N2 for the three gases have undergone significant changes, and the adsorption performance of the system has increased. This also validates the necessity of our work.

4. Conclusion

This work systematically investigates the adsorption behaviors and interfacial interaction mechanisms of three typical insulation decomposition gases (CH_4, C_2N_2, and CO_2) on the surface of Cr-decorated C_3N_2 monolayer materials based on Density Functional Theory (DFT). Results show that Cr-C_3N_2 exhibits significant adsorption selectivity differences toward the three types of gases: strong chemisorption for C_2N_2 (-2.148 eV), weak chemisorption for CO_2 (-0.866 eV), and predominantly physisorption for CH_4 (-0.305 eV). By integrating charge transfer analysis, differential electron density calculations, and work function evolution studies, the bonding characteristics and electron transfer rules between gas molecules and the substrate are revealed. Specifically, C_2N_2 induces significant charge transfer (ΔQ=0.034 e) through Cr-N covalent bonding, while CO_2 adsorption primarily relies on Cr-O polar interactions. Density of states (DOS) analysis further clarifies the hybridization mechanism between Cr-3d orbitals and gas molecular orbitals, confirming strong orbital coupling in the C_2N_2 adsorption system. This research provides theoretical support for the application of novel two-dimensional nitride materials in the field of insulation fault gas detection and processing in power equipment, while deepening the understanding of microscale gas-sensing mechanisms.

Abbreviations

DFT	Density Functional Theory
Cr-C_3N_2	Cr Atom Doping Modification of C_3N_2 Base
E_{ads}	Adsorption Energy
E_b	System Binding Energy
ΔQ	Charge Transfer
GIS	Gas Insulated Switchgear
GIL	Gas Insulated Metal-enclosed Transmission Line
DOS	Density of States
TDOS	Total Density of States
PDOS	Partial Density of States

Author Contributions

Tao Wang: Conceptualization, Investigation, Software, Writing – original draft

Xuchu Hu: Data curation, Investigation, Methodology

Huan Yang: Formal Analysis, Software, Validation

Lei Chen: Data curation, Software, Validation

Jianjun Cao: Data curation, Methodology, Resources, Software, Writing – original draft, Writing – review & editing

Pengfei Jia: Funding acquisition, Resources, Supervision, Writing – review & editing

Yiyi Zhang: Methodology, Supervision, Visualization, Writing – original draft

Funding

This work is supposed by Technology Development Projects of Guangxi Liuzhou Special Transformer Co., Ltd., and Project for Enhancing Young and Middle-aged Teacher's Research Basis Ability in Colleges of Guangxi (Research on high precision detection of local discharge in high voltage switch cabinet based on sensing modulation and deep learning, Grant No. 2025KY0042).

Conflicts of Interest

The authors declare no conflicts of interest.

References

[1] Huang, H., Yu, Y., Zhang, M., 2020. Analysis of adsorption properties of SF_6 decomposed gases (SOF_2, SO_2F_2, SF_4, CF_4, and HF) on Fe-doped SWCNT: A DFT study. Appl. Surf. Sci. 505, 144622. https://doi.org/10.1016/j.apsusc.2019.144622

[2] Li, B., Zhou, Q., Peng, R., Liao, Y., Zeng, W., 2021. Adsorption of SF_6 decomposition gases (H_2S, SO_2, SOF_2 and SO_2F_2) on Sc-doped MoS_2 surface: A DFT study. Appl. Surf. Sci. 549, 149271. https://doi.org/10.1016/j.apsusc.2021.149271

[3] Ye, F., Zhang, X., Li, Y., Wan, Q., Bauchire, J.-M., Hong, D., Xiao, S., Tang, J., 2022. Arc decomposition behavior of C_4F_7N/Air gas mixture and biosafety evaluation of its by-products. High Volt. 7, 856–865. https://doi.org/10.1049/hve2.12233

[4] Sang, T.-Y., Sun, H., Hu, X., Li, T., Guo, L.-Y., Peng, Z., Wang, G., Zhu, C., Zou, S., Zhang, X., Wang, S., Li, W., Chen, W., 2022. 38Theoretical Exploration of C_4F_7N Decompositions on GeSe Monolayers for Gas Sensing Based on DFT Method. IEEE Sens. J. 22, 13915–13920. https://doi.org/10.1109/JSEN.2022.3184033

[5] Gao, W., Posada, L., Shiravand, V., Shubhashish, S., Price, C., Zhang, B., Potyrailo, R., Younsi, K., Shan, S., Ndiaye, I., Cabrera, C., Zhou, J., Perret, M., Berteloot, T., Kieffel, Y., Laso, A., Uzelac, N., Suib, S. L., Cao, Y., 2024. Decomposition characteristics of C_4F_7N-based SF_6-alternative gas mixtures. J. Appl. Phys. 135, 063302. https://doi.org/10.1063/5.0188478

[6] Jia, P., Cao, J., Wang, M., Zhang, Y., Liu, J., Xu, M., Chen, D., 2024. Exploration of SF_6 and its decomposed gases in adsorption and sensing (four modified WSe_2 monolayers at quantum level). Surf. Interfaces 51, 104606. https://doi.org/10.1016/j.surfin.2024.104606

[7] Guo, G., Mao, L., Liu, K., Tan, X., 2024. Pd-Adsorbed SiN_3 Monolayer as a Promising Gas Scavenger for SF_6 Partial Discharge Decomposition Components: Insights from the First-Principles Study. Langmuir 40, 7669–7679. https://doi.org/10.1021/acs.langmuir.4c00370

[8] Cui, H., Zhu, H., Jia, P., 2020. Adsorption and sensing of SO_2 and SOF_2 molecule by Pt-doped $HfSe_2$ monolayer: A first-principles study. Appl. Surf. Sci. 530, 147242. https://doi.org/10.1016/j.apsusc.2020.147242

[9] Zhang, X., Chen, D., Cui, H., Dong, X., Xiao, S., Tang, J., 2017. Understanding of SF_6 decompositions adsorbed on cobalt-doped SWCNT: A DFT study. Appl. Surf. Sci. 420, 371–382. https://doi.org/10.1016/j.apsusc.2017.05.163

[10] Vessally, E., Hosseinali, Mehdi, Poor Heravi, Mohammad Reza, and Mohammadi, B., 2023. DFT study of the adsorption of simple organic sulfur gases on g-C_3N_4; periodic and non-periodic approaches. J. Sulfur Chem. 44, 733–750. https://doi.org/10.1080/17415993.2023.2209687

[11] Xu, X.-Y., Xu, H., Guo, H., Zhao, C., 2020. Mechanism investigations on CO oxidation catalyzed by Fe-doped graphene: A theoretical study. Appl. Surf. Sci. 523, 146496. https://doi.org/10.1016/j.apsusc.2020.146496

[12] Wang, J.-H., Lin, M. C., 2004. Adsorption and Reaction of C_2N_2 on Si(100)-2 × 1: A Computational Study with Single- and Double-Dimer Cluster Models. J. Phys. Chem. B 108, 9189–9197. https://doi.org/10.1021/jp0495343

[13] Alamri, S., Rajhi, Ali A., and Derakhshande, M., 2022. Potential detection of C_2N_2 gas by the pure, Al, and Cu-doped graphynes: a DFT study. Mol. Simul. 48, 574–583. https://doi.org/10.1080/08927022.2022.2036338

[14] Khatun, M., Rocky, M. H., Roman, A. A., Roy, D., Badsha, Md. A., Ahmed, M. T., 2025. Impact of N-Doping on $MoSe_2$ Monolayer for PH_3, C_2N_2, and HN_3 Gas Sensing: A DFT Study. ChemistryOpen 14, e202400210. https://doi.org/10.1002/open.202400210

[15] Zhao, H., He, X., Shi, Z., Li, S., 2024. Adsorption and sensing behavior of Cr-doped WS_2 monolayer for hazardous gases in agricultural greenhouses: A DFT study. Mater. Today Commun. 40, 109405. https://doi.org/10.1016/j.mtcomm.2024.109405

[16] Hu, Y., Wang, L., Nan, R., Xu, N., Jiang, Y., Wang, D., Yan, T., Liu, D., Zhang, Y., Chen, B., 2023. Pore engineering in cost-effective and stable Al-MOFs for efficient capture of the greenhouse gas SF_6. Chem. Eng. J. 471, 144851. https://doi.org/10.1016/j.cej.2023.144851

[17] Zhang, J., Feng, W., Zhang, Y., Zeng, W., Zhou, Q., 2023. Gas-sensing properties and first-principles comparative study of metal (Pd, Pt)-decorated MoSe2 hierarchical nanoflowers for efficient SO2 detection at room temperature. J. Alloys Compd. 968, 172006. https://doi.org/10.1016/j.jallcom.2023.172006

[18] Baildya, N.; Mazumdar, S.; Mridha, N. K.; Chattopadhyay, A. P.; Khan, A. A.; Dutta, T.; Mandal, M.; Chowdhury, S. K.; Reza, R.; Ghosh, N. N. Comparative Study of the Efficiency of Silicon Carbide, Boron Nitride and Carbon Nanotube to Deliver Cancerous Drug, Azacitidine: A DFT Study. Comput. Biol. Med. 2023, 154, 106593. https://doi.org/10.1016/j.compbiomed.2023.106593

[19] Chen, H.; Guo, Y.; Zhou, K.; Wang, J.; Zeng, Z.; Li, L. Mechanism Exploration of Surface Functional Groups and Pore Sizes on CO_2 Adsorptive Separation by GCMC and DFT Simulations. Sep. Purif. Technol. 2023, 318, 123993. https://doi.org/10.1016/j.seppur.2023.123993

[20] Zhang, H.; Zhou, W.; Jiang, J.; Zeng, W.; Zhou, Q. First-Principles Investigation of Transition Metal (Co, Rh, and Ir)-Modified WS_2 Monolayer Membranes: Adsorption and Detection of SF_6 Decomposition Gases. ACS Appl. Nano Mater. 2024, 7 (11), 13379–13391. https://doi.org/10.1021/acsanm.4c01791

[21] Xu, L., Zhu, H., Gui, Y., Long, Y., Wang, Q., Yang, P., 2020. First-Principles Calculations of Gas-Sensing Properties of Pd Clusters Decorated AlNNTs to Dissolved Gases in Transformer Oil. IEEE Access 8, 162692–162700. https://doi.org/10.1109/ACCESS.2020.3020636

[22] Yin, X.-T., Liu, Y., Tan, X.-M., Gao, X.-C., Li, J., Ma, X., 2022. New Analysis Method for Adsorption in Gas (H_2, CO)–Solid (SnO_2) Systems Based on Gas Sensing. ACS Omega 7, 21262–21266. https://doi.org/10.1021/acsomega.2c02405

[23] Cao, J.; Wang, M.; Zhang, Y.; Liu, J.; Xu, M.; Chen, D.; Jia, P. Gas Sensitivity Evaluation of Decomposition Gases in Environmentally Friendly Insulating Devices (C_4F_7N/CO_2) (Chromium Cluster-Modified BNNTs Surface Interface at the Atomic Scale). Surf. Interfaces 2024, 54, 105202. https://doi.org/10.1016/j.surfin.2024.105202

[24] Yu, W.; Zhu, Y.; Zhao, J.; Zhu, P. DFT-Based Adsorption Studies of CNCl, HCN, and NH_3 on Metal-Doped Diamane. Appl. Surf. Sci. 2024, 670, 160672. https://doi.org/10.1016/j.apsusc.2024.160672

[25] Cui, Z., Yang, K., Shen, Y., Yuan, Z., Dong, Y., Yuan, P., Li, E., 2023. Toxic gas molecules adsorbed on intrinsic and defective WS_2: gas sensing and detection. Appl. Surf. Sci. 613, 155978. https://doi.org/10.1016/j.apsusc.2022.155978

[26] Wang, R., Cheng, B., Ou, W., 2023. 48Intrinsic and Ag-doped graphdiyne as a two-dimensional material gas sensing detector for the detection of SF_6 decomposition products. Appl. Surf. Sci. 608, 155276. https://doi.org/10.1016/j.apsusc.2022.155276

[27] Zhu, J., Zhang, H., Tong, Y., Zhao, L., Zhang, Y., Qiu, Y., Lin, X., 2017. First-principles investigations of metal (V, Nb, Ta)-doped monolayer MoS_2: Structural stability, electronic properties and adsorption of gas molecules. Appl. Surf. Sci. 419, 522–530. https://doi.org/10.1016/j.apsusc.2017.04.157

[28] Bals, S., Marin, G. B., Detavernier, C., Dendooven, J., 2019. Chemical and Structural Configuration of Pt-Doped Metal Oxide Thin Films Prepared by Atomic Layer Deposition. Chem. Mater. 31, 9673–9683. https://doi.org/10.1021/acs.chemmater.9b03066

[29] Peter, C. N., Anku, W. W., Shukla, S. K., Govender, P. P., 2018. Theoretical studies of the interfacial charge transfer and the effect of vdW correction on the interaction energy of non-metal doped ZnO and graphene oxide interface. Theor. Chem. Acc. 137, 75. https://doi.org/10.1007/s00214-018-2258-4

[30] Liu, Z., Gui, Y., Xu, L., Chen, X., 2022. Adsorption and Sensing Performance of Transition Metal (Ag, Pd, Pt, Rh, and Ru) Modified WSe_2 Monolayer for SF_6 Decomposition Gases (SOF_2 and SO_2F_2). Appl. Surf. Sci. 581, 152365. https://doi.org/10.1016/j.apsusc.2021.152365

[31] Zhang, X., Qiao, H., Sun, H., Wang, P., Tao, L.-Q., 2023. Adsorption of SF_6 gas and insulating oil decomposition gas by CoO-doped SnSe monolayer in various environments: A study of strong adsorption performance. Chem. Phys. 573, 112001. https://doi.org/10.1016/j.chemphys.2023.112001

[32] Ueda, T., Boehme, I., Hyodo, T., Shimizu, Y., Weimar, U., Barsan, N., 2021. Effects of Gas Adsorption Properties of an Au-Loaded Porous In_2O_3 Sensor on NO_2-Sensing Properties. ACS Sens. 6, 4019–4028. https://doi.org/10.1021/acssensors.1c01412

[33] Peng, W., Guo, Y., Zhang, Y., Wu, W., Liu, Y., Zhou, Z., 2020. A first-principles investigation of double transition metal atoms embedded C_2N monolayer as a promising SF_6 gas adsorbent and scavenger. Mater. Chem. Phys. 240, 122184. https://doi.org/10.1016/j.matchemphys.2019.122184

[34] Galstyan, V., Moumen, A., Kumarage, G. W. C., Comini, E., 2022. Progress towards chemical gas sensors: Nanowires and 2D semiconductors. Sens. Actuators B Chem. 357, 131466. https://doi.org/10.1016/j.snb.2022.131466

[35] Cao, J., Wang, M., Zhang, Y., Liu, J., Chen, D., Jia, P., 2024. CoO-SnSe monolayer: A high potential candidate for SF_6 characteristic decomposition gas adsorption and detection. Colloids Surf. Physicochem. Eng. Asp. 688, 133671. https://doi.org/10.1016/j.colsurfa.2024.133671

[36] Salih, E., Ayesh, A. I., 2021. Pt-doped armchair graphene nanoribbon as a promising gas sensor for CO and CO_2: DFT study. Phys. E Low-Dimens. Syst. Nanostructures 125, 114418. https://doi.org/10.1016/j.physe.2020.114418

[37] Wang, M., Zhou, Q., Zeng, W., 2022. Theoretical study on adsorption of SF_6 decomposition gas in GIS gas cell based on intrinsic and Ni-doped $MoTe_2$ monolayer. Appl. Surf. Sci. 591, 153167. https://doi.org/10.1016/j.apsusc.2022.153167

[38] Zhu, J., Zins, E.-L., Alikhani, M. E., 2018. Dehydrocoupling of dimethylamine borane by titanocene: elucidation of ten years of inconsistency between theoretical and experimental descriptions. Phys. Chem. Chem. Phys. 20, 15687–15695. https://doi.org/10.1039/C8CP01970C

[39] Jia, P., Qiao, S., Wang, Y., Liu, Y., 2021. Pd-decorated GaN monolayer as a promising scavenger for SO_2 and SOF_2 in SF6 insulation equipment: A first-principles study. Comput. Theor. Chem. 1201, 113276. https://doi.org/10.1016/j.comptc.2021.113276

[40] Diao, Y., Liu, L., Xia, S., 2018. Adsorption of residual gas molecules on (10–10) surfaces of pristine and Zn-doped GaAs nanowires. J. Mater. Sci. 53, 14435–14446. https://doi.org/10.1007/s10853-018-2610-z

[41] Deng, P., Cheng, L., Jiang, P., Zeng, Z., Li, A., Liao, C., 2022. Sensing performance of CdPc monolayer toward the SF_6 decomposition gases: A DFT study. Chem. Phys. Lett. 806, 140030. https://doi.org/10.1016/j.cplett.2022.140030

[42] Zhang, Q., Gui, Y., Qiao, H., Chen, X., Cao, L., 2022. Theoretical study of SF_6 decomposition products adsorption on metal oxide cluster-modified single-layer graphene. J. Ind. Eng. Chem. 105, 278–290. https://doi.org/10.1016/j.jiec.2021.09.025

[43] Sun, M.; Chen, M.; Cui, X.; Zhao, Z.; Wang, J.; Liang, L.; Zhou, Y. Unveiling the Gas Sensing Potential of CxNy Monolayer through Ab Initio Screening. Surf. Interfaces 2023, 42, 103313. https://doi.org/10.1016/j.surfin.2023.103313

[44] Zeng, L.; Zhang, Z.; Zhou, C.; Liao, M.; Sun, C. Molecular Dynamics Simulation and DFT Calculations on the Oil-Water Mixture Separation by Single-Walled Carbon Nanotubes. *Appl. Surf. Sci.* 2020, *523*, 146446. https://doi.org/10.1016/j.apsusc.2020.146446

[45] Zhao, C.; Zhang, W.; Zhang, Y.; Yang, Y.; Guo, D.; Liu, W.; Liu, L. Influence of Multivalent Background Ions Competition Adsorption on the Adsorption Behavior of Azo Dye Molecules and Removal Mechanism: Based on Machine Learning, DFT and Experiments. Sep. Purif. Technol. 2024, 341, 126810. https://doi.org/10.1016/j.seppur.2024.126810

[46] Wang, T., Hu, X., Yang, H., Chen, L., Cao, J., Jia, P., Zhang, Y., 2025. Design of Pt-C_3N_2 composites for efficient real-time monitoring of fluorocarbon insulation gas decomposition and its application in GIS equipment. Surf. Interfaces 68, 106721. https://doi.org/10.1016/j.surfin.2025.106721